Meteorologische Zeitschrift, PrePub DOI 10.1127/metz/2015/0625
© 2015 The authors

Open Access Article

Characterisation and predictability of a strong and a weak forcing severe convective event – a multi-data approach

Kathrin Wapler[1,2*], Florian Harnisch[2,3], Tobias Pardowitz[2,4] and Fabian Senf[2,5]

[1]Deutscher Wetterdienst, Offenbach, Germany
[2]Hans-Ertel-Centre for Weather Research, Offenbach, Germany
[3]Ludwig-Maximilians-Universität München, Germany
[4]Freie Universität Berlin, Germany
[5]Leibniz Institute for Tropospheric Research, Leipzig, Germany

(Manuscript received June 20, 2014; in revised form October 24, 2014; accepted December 21, 2014)

Abstract

Two severe summer-time convective events in Germany are investigated which can be classified by the prevailing synoptic conditions into a strong and a weak forcing case. The strong forcing case exhibits a larger scale precipitation pattern caused by frontal ascent whereas scattered convection is dominating the convective activity in the weak forcing case. Other distinguished differences between the cases are faster movement of convective cells and larger regions with significant loss mainly due to severe gusts in the strong forcing case. A comprehensive set of various observations is used to characterise the two different events. The observations include measurements from a lightning detection network, precipitation radar, geostationary satellite and weather stations, as well as information from an automated cell detection algorithm based on radar reflectivity which is combined with severe weather reports, and damage data from insurances. Forecast performance at various time scales is analysed ranging from nowcasting and warning to short-range forecasting. Various methods and models are examined, including human warnings, observation-based nowcasting algorithms and high-resolution ensemble prediction systems. The analysis shows the advantages of a multi-sensor and multi-source approach in characterising convective events and their impacts. Using data from various sources allows to combine the different strengths of observational data sets, especially in terms of spatial coverage or data accuracy, e.g. damage data from insurances provide good spatial coverage with little meteorological information while measurements at weather stations provide accurate but pointwise observations. Furthermore, using data from multiple sources allow for a better understanding of the convective life cycle. Several parameters from different instruments are shown to have a predictive skill for convective development, these include satellite-based cloud-top cooling rates as measure for intensive convective growth, 3D-radar reflectivity, mesocyclone detection from doppler radar, overshooting top detection or lightning jumps to evaluate storm intensification and formation of severe weather. This synergetic approach can help to improve nowcasting algorihtms and thus the warning process. The predictability of the analysed severe convective events differs with different types of forcing which is reflected in both, convective-scale ensemble prediction system forecasts and human weather warnings. Human warnings show larger false alarm rates in the weak forcing case. Ensemble predictions are able to capture the characteristics of the convective precipitation. The forecast skill is connected strongly to the synoptic situation and the presence of large-scale forcing increases the forecast skill. This has to be considered for potential future warn-on-forecast strategies.

Keywords: deep convection, observations, warnings, nowcasting, high-resolution ensemble modeling

1 Introduction

Severe weather associated with thunderstorms poses a significant threat to life, property and economy. Hence, the detailed knowledge, early detection and improved forecasting of the occurrence of thunderstorms and their characteristics is important particularly to enable weather services to provide appropriate and timely warning information to their users. Wapler (2013) present a detailed thunderstorm climatology for Central Europe. A better understanding of the underlying thermodynamic process of thunderstorm development may improve forecasting of such events. The formation of (severe) convective weather events depends on a variety of processes. While fast processes on the mesoscale are responsible for the impact itself, it is the synoptic situation, associated with slow processes, that creates the environment for such events. Wapler and James (2014) examine the thunderstorm distribution in relation to synoptic conditions. Their analysis reveals conditions favourable for thunderstorm development and highlights regions affected under different flow regimes. Additionally, different synoptic conditions are typically associated with specific cell characteristics such as the direction and speed of movement, size and severity.

One of the major challenges in nowcasting severe convection is the early detection of convective initi-

*Corresponding author: Kathrin Wapler, Hans-Ertel-Centre for Weather Research, Atmospheric Dynamics and Predictability Branch, Deutscher Wetterdienst, Offenbach, Germany, e-mail: kathrin.wapler@dwd.de

© 2015 The authors

ation (CI) and characterisation of convective growth by remote sensing networks. For large domains, multispectral imagery from geostationary satellites has been used to improve CI detections (Mecikalski and Bedka, 2006; Mecikalski et al., 2010; Siewert et al., 2010) and to estimate vertical growth rates (Sieglaff et al., 2011). It was shown that developing cumulus clouds may be observed from satellite with a lead time of 15–60 min before precipitation formation (Siewert et al., 2010). The life cycle of satellite-derived cloud-top properties in convective development was further investigated in e.g. Mecikalski et al. (2011); Horvath et al. (2012); Cintineo et al. (2013); Senf et al. (2015). It was shown that vertical growth rates and horizontal anvil expansion is significantly larger for severe storms. Furthermore, changes in lightning frequency were related to satellite-derived cloud-top properties.

The predictability of convective events is bounded by the rapid error growth and nonlinearity at the convective-scale resolution (Hohenegger and Schär, 2007; Selz and Craig, 2014) and often limited to a few hours. Large-scale flow characteristics can have a considerable effect on the predictability. Various studies have shown that in the absence of a synoptic forcing mechanism of the convection, the forecast performance is often bad and the predictability is reduced (Trentmann et al., 2009; Barthlott et al., 2011). In this case, the convective precipitation pattern is often controlled by atmospheric boundary layer processes and orography. On the contrary, the presence of a large-scale synoptic forcing can increase the predictability of convective precipiation (Keil et al., 2014). To improve forecasts of convective events, ensemble forecasts with high horizontal resolution are now frequently produced. The convective-scale ensemble prediction system (EPS) of the Deutscher Wetterdienst (DWD) COSMO-DE-EPS computes 21 h ensemble forecasts at a grid resolution of 2.8 km over Germany which are updated every 3 hours. The forecast ensemble consists of 20 ensemble members using perturbations of the initial conditions, the lateral boundary conditions and the model physics (Gebhardt et al., 2011; Peralta et al., 2012; Kühnlein et al., 2014).

The warning strategy of the Deutscher Wetterdienst (DWD) includes a 3 stage warning management, based on the concept of a progressive spatial and temporal refinement (Weingaertner et al., 2009). The actual warnings are issued on district level and need to take into account the conflictive needs of users to obtain timely and precise warnings. Current practice in this respect is a "warn on observation" strategy with accordingly short lead times. Based on probabilistic evidence, however, future development at the Deutscher Wetterdienst may be directed towards a "warn on forecast" strategy (Stensrud et al., 2009). The synergetic combination of modern observational network data and convection-permitting modelling seems to be the most promising way to establish probabilistic forecasts (Kain et al., 2013).

During the field campaign COPS (Convective and Orographically-induced Precipitation Study) a synergy of in-situ and remote sensing measurement systems was employed in the low mountain regions of Southwestern Germany and Eastern France. The field campaign and related modelling studies provide new insights into processes leading to convection initiation, to the modification of precipitation by orography, and in the performance of ensembles of convection-permitting models in complex terrain (Wulfmeyer et al., 2008). However, such synergetic approaches to the characterisation of atmospheric convection have usually been confined to small domains at specific observation sites.

In the present study, two synoptically different convective storm events are evaluated over Germany which are classified as severe events (see Table 1 for an overview). The events are studied with a synergetic approach, bringing together observations and measurements of meteorological phenomena with the impact of the events, operational warnings, observation-based nowcasting, numerical weather prediction and information accessed by the public.

Relying on single data sources may lead to an incomplete picture due to limitations in the individual data sets or model errors. Verifying severe weather warnings, difficulties may arise due to a lack of extensive observational data and imperfect observation systems (Smith, 1999). Loss insurance records provide additional valuable information on severe weather conditions and complement punctually available observational data. This is particularly the case for local-scale characteristics of thunderstorms and hail occurrence (Kunz and Puskeiler, 2010; Schuster et al., 2006; Hohl et al., 2002). This study demonstrates the benefit of a combined analysis of different data sets and forecast systems for the characterisation of severe weather events. Furthermore, the manifoldness of aspects involved in the assessment of forecast quality and in the quantification of impacts related to severe weather conditions are shown. The study aims to address aspects which potentially need to be improved in the forecasting chain to possibly achieve an overall improvement of forecast quality necessary for successful and effective warning of severe weather in situations with different predictability.

In summary, the objectives of the present study are to (a) identify possible synergies of considering different data sources which may enable a better understanding and characterisation of local severe weather events, (b) possibly indicate shortcomings or weak spots in the meteorological forecasts and warning process and (c) assess the predictability for synoptically different convective events.

The remainder of this paper is organised as follows. In Section 2 the used data sets and models are described. Sections 3 and 4 present in detail the strong forcing frontal case and the weak forcing case, respectively. A comparison of the cases is discussed in Section 5.

Table 1: Overview of warnings, information access by the public, observations and impacts of the two cases.

Category	6 June 2011	22 June 2011	reference
losses in EUR	24.5 Mio	52.9 Mio	
loss ratio Germany-wide	43th highest	18th highest	summer 1997–2011
loss ratio in most damaged county	highest	2nd highest	summer 1997–2011
ESWD hail diameter maximum (cm)	7.2	3.5	
ESWD tornado intensity	F0	F1	
number of ESWD gust reports	1 (QC0+) and 8 (QC1)	8 (QC0+) and 140 (QC1)	
number of ESWD hail reports	13 (QC0+) and 11 (QC1)	7 (QC0+)	
number of ESWD tornado reports	1 (QC1)	3 (QC1)	
strongest gust at 5 synop stations	$\geq$ 76 km/h	$\geq$ 100 km/h	
heaviest precipitation (mm/day)	71.0	46.4	
highest rain rate (mm/h)	53.5	35.4	
number of warnings per day	99 % percentile	95 % percentile	04/2003–12/2012
number of webpage access per day	99 % percentile	97 % percentile	summer 2008–2013
number of warning webpage access per day	85 % percentile	96 % percentile	summer 2008–2013

Finally, Section 6 provides a summary and some concluding remarks.

2 Data and methods

2.1 Impact data

Insurance data on losses to residential buildings are collected by the German insurance association (Gesamtverband der Deutschen Versicherungswirtschaft e.V., GDV). These comprise daily data on administrative district level. In contrast to point-wise measurements from meteorological stations, the available insurance data represent measurements with an area-wide coverage of wind storm and thunderstorm losses. These data have been evaluated in several weather impact studies (Donat et al., 2011; Held et al., 2013).

The quantity loss ratio is commonly used by insurances and is defined as the loss (in EUR) divided by the insured sum (in thousand EUR) which is thus specified in (= 1EUR/1000EUR). Besides ensuring spatial homogenization, the consideration of relative losses removes temporal inhomogeneities resulting e.g., from value enhancement or inflation.

Additionally, hail, gust and tornado reports of the European Severe Weather Database (ESWD, Dotzek et al. (2009), Dotzek and Groenemeijer (2009), Groenemeijer et al. (2009)) are used. The ESWD hail data set contains events with hailstones having a diameter of 2 cm or more, or smaller hailstones that form a layer of at least 2 cm thickness on flat parts of the earth's surface. Further, the data base includes severe wind gusts that in order to be recorded are required to have a measured wind speed of at least 25 m/s or to cause such damage that a wind speed of 25 m/s or higher is likely to have occurred. A vortex typically between a few metres to a few kilometres in diameter, extending between a convective cloud and the earth's surface, that may be visible by condensation of water and/or by material that is lifted off the earth's surface is classified as tornado according to the ESWD. The database includes information of the location (latitude/longitude) and time (with an uncertainty estimate) of the event, a quality control flag and for some cases some additional information such as hail size.

A three-level quality-control is applied to all reports of the ESWD. The QC-levels have the following meaning: QC0: "as received", QC0+: "plausibility checked", QC1: "report confirmed" by reliable sources and QC2: "event fully verified" i.e. all information about this event is verified, consistent and comes from reliable sources. For this study, data with quality flags QC1 and QC2 is used.

2.2 Measurements

Observations of the about 260 German surface stations measuring wind gusts and of 1205 stations measuring precipitation are analysed. The datasets provide hourly maximum gusts as well as hourly rain rates.

The DWD operates a network of 16 radar stations using C-Band Doppler radars evenly distributed over Germany. The radar stations run continuously in operational mode and provide complete volume scans every 15 minutes during the time of the events, which has been updated to 5 minutes. 2D-scans, the so-called precipitation scans, are accomplished every 5 minutes.

Lightning measurements are provided by the European LIghtning detection NETwork LINET (Betz et al., 2009). The lightning network consist of 30 antennas in Germany and many more in Europe. It is considered to have a very high detection efficiency with a quasi continuous spatial and temporal resolution. Stroke location (latitude/longitude) and some attributes are provided in real time with no discretisation on any spatial or tempral grid. According to comparisons with measurements on towers, whose positions are well known, the stroke location accuracy is estimated to be in the order of 100 m.

The radiometer SEVIRI aboard the geostationary satellites of Meteosat Second Generation (MSG) operating in Rapid Scan Mode provides infrared and visible

images with a horizontal resolution of 3 to 5 km each 5 minutes. They are analysed and used for the characterisation of cloud-top properties and their temporal changes.

2.3 Nowcasting algorithms

The automated cell detection algorithm KONRAD (*KONvektionsentwicklung in RADarprodukten*, convection evolution in radar products, Lang (2001)) uses 2D radar reflectivity data. It runs operationally every 5 minutes. KONRAD uses a threshold for the detection of a cell of 46 dBZ in an area of 15 km^2. The system provides the location of a cell along with some additional cell information. These cell attributes include the movement speed and direction of the cell, the size of the cell with equal or more than 46 dBZ and the size of the area of more than 55 dBZ within the detected cell. From the lightning data, the number of strokes within 15 km of the cell center has been calculated. Some verification results can be found in Wapler et al. (2012).

Algorithms using 3D doppler radar data are able to detect mesocyclones (Zrnic et al., 1985). The algorithm operationally used at DWD (Hengstebeck et al., 2011) is analysed in the present study.

Based on a combination of MSG-SEVIRI brightness temperatures from the 10.8 µm channel and reflectances from a high-resolution visible channel, convective cells are manually tracked. Cloud-top cooling rates are derived from along-track 5 min time trends of infrared brightness temperatures and uncertainties are estimated from spatial variations of cloud-top properties. Furthermore, overshooting tops are identified by the simultaneous occurrence of local minima in the cloud-top temperature with values below 220 K and large gradients in the visible reflectances resulting from the difference in illuminated and shaded parts of the convective cloud tower.

2.4 Warnings

The warning strategy of the DWD comprises a three-step warning management with early warning, pre-warning and detailed district based warnings in accordance to the principle of progressive spatial and temporal refinement. Early warning information is issued in the form of a warning report covering the upcoming week, containing probabilistic information (possible, likely and very likely) about expected significant weather events on a nationwide spatial scale (250–700 km). Preliminary warning information is given at least 24 hours in advance considering significant weather events on a regional scale (50–250 km). Detailed severe weather warnings are issued on district level with lead times balancing the users conflicting needs for timely and precise information. For thunderstorm events warning lead times range between 0 to 3 hours and they are typically issued for a duration of 3 to 6 hours.

2.5 Convective-scale short-range forecasts

Convective-scale forecasts are produced with the high-resolution limited area COSMO-DE model (Baldauf et al., 2011) on a operational basis at DWD since 2007. The COSMO-DE model uses a rotated latitude-longitude grid that consists of 461 × 421 grid points with a horizontal resolution of 2.8 km and 50 vertical levels. The domain covers Germany and parts of the neighboring countries in Central Europe. Only shallow convection is parametrised in COSMO-DE, but deep convection is resolved explicitly. COSMO-DE forecasts are initialised from a high-resolution analysis which assimilates radar data via a latent heat nudging method into the model (Stephan et al., 2008) and 21 h forecasts are computed every 3 hours. For more details on the COSMO-DE forecast model please refer to Baldauf et al. (2011).

The COSMO-DE-EPS is based on the COSMO-DE model, but instead of just one deterministic forecast now several parallel ensemble forecasts are computed. The forecast lead time, update and resolution is the same as for the deterministic run and forecasts with 21 h lead time are issued every 3 hours. To represent uncertainty which stems from the lateral boundaries of the domain, COSMO-DE-EPS is driven by a set of four different lateral boundary conditions (LBCs) which are provided by forecasts from a four member COSMO-EU ensemble with 7 km grid resolution (namely BC-EPS). Each of the four BC-EPS members is nested into a different global model, which are the ECMWF IFS model, the DWD GME model, the JMA GSM model and the NCEP GFS model.

Additionally, initial uncertainty on the convective-scales also affects the forecasts and there is a clear benefit of explicitly accounting for the initial uncertainty especially at shorter lead times up to 12 hours (Vié et al., 2011; Kühnlein et al., 2014). A method to perturb the initial conditions has been developed for COSMO-DE-EPS, which is based on a downscaling approach (Peralta et al., 2012). It uses the information of the four member BC-EPS to compute a set of four perturbations which are added to the deterministic COSMO-DE analysis to provide four different initial ensembles with each having five members. Each of the four sets of five ensemble members applies perturbations to the default values of five constant parameters of the model physics parametrizations to account for model uncertainty during the forecast integration (Gebhardt et al., 2011). This creates a 20 member COSMO-DE-EPS forecast.

3 The strong forcing case: 22 June 2011

3.1 Synoptic overview

The synoptic pattern on 22 June 2011 can be classified as Cyclonic Westerly (Wz) according to James (2007). A mid/upper-level trough was situated over the

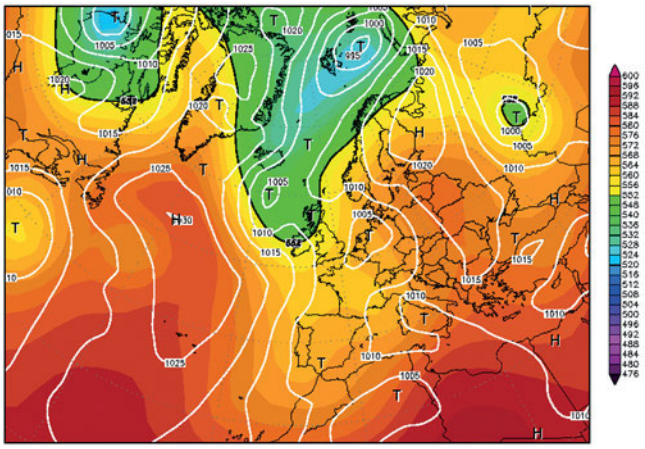

Figure 1: 500 hPa geopotential and surface pressure on 00:00 UTC 22 June 2011. Taken from www.wetterzentrale.de.

UK and Ireland (Fig. 1). Within a strong westsouthwesterly flow over western Europe, a shortwave trough translated rapidly northeastward during the day. This system was preceded by a well-developed cold front, along which a baroclinic wave developed. The front separated warm moist unstable subtropical air in the South and South-East from cooler maritime air in the North-West. A widespread, homogeneous region with intense precipitation can be observed from 12:00 UTC until about 18:00 UTC when the system moves out of Germany (Fig. 2a–c). South-East of this system further convective cells developed – mainly orographically induced – that propagated northeastwards. Using the convective adjustment time-scale (Done et al., 2006; Keil et al., 2014; Zimmer et al., 2011) as an indicator, 22 June 2011 is classified as a case with strong synoptic forcing. The area averaged convective adjustment time scale over Germany does not exceed 5 hours.

Five days ahead on 17 June 2011, the (human) forecast predicted that thunderstorms with heavy rain, strong gusts and hail are likely for the South and East of Germany. Three days ahead on 20 June 2011, the human forecasters indicated the potential for severe weather occurring on 22 June 2011.

3.2 Short-range forecast

The deterministic and ensemble COSMO-DE forecasts both correctly predict the cold front passage over Germany during the afternoon of the 22 June 2011 (Fig. 2). The North-South orientated band with intense rain moves across the domain towards the East and the precipitation along the Northern Alps is also predicted. COSMO-DE-EPS predicts high probabilities of rain around the location of the frontal structure. High probabilities of rain are generally dominating the forecasts and the ensemble predictions show only little uncertainty about the location of the rain bands. However, this could also be related to the ensemble forecast being under dispersive.

The domain averaged precipitation over Germany for the strong-forcing case (Fig. 3a) shows a distinct peak in the afternoon when the cold front was located over Germany. Both forecasts, deterministic and ensemble mean, and observations are giving similar precipitation amounts at early times with a slight tendency to underestimate the precipitation in the afternoon. The occurrence of the maximum during the afternoon is predicted correctly, but some problems connected to the timing of the cold front are apparent. The forecasted precipitation maximum occurs slightly later than the observed one and too large precipitation amounts are predicted after the maximum from 17:00 UTC onwards.

Fig. 3 shows also the results for the single COSMO-DE-EPS members separated with respect to their BC-EPS driven by the corresponding global model. The ensemble members cluster strongly with respect to their corresponding BC-EPS member the impact of the corresponding BC-EPS is large (Fig. 3a). In the strong forcing case, the precipitation location and intensity is determined by the propagating cold front. The different global models have a different timing in the precipitation entering the domain and during the first forecast hours the ensemble members of different driving BC-EPS are strongly split up. Further, differences between the ensemble members are found for the maximum precipiation during the afternoon. The ensemble members slightly underestimate the precipitation during the peak precipitation period in the late afternoon up to 12 h forecast lead time. From 15 h onwards, when the cold front propagates out of the domain in the East, all forecast overestimate the precipitation due to a too slow propagation of the cold front. The observed area average precipitation diminishes after 17 h forecast lead time (Fig. 3a), which leads to large biases in the precipitation forecasts.

For the detection of severe convective rotating cells in model simulations the supercell detection index (SDI) can be calculated (Wicker et al., 2005; Baldauf and Seifert, 2008). The 00:00 UTC forecast of COSMO-DE-EPS reveals clear signals of SDI associated with the front (not shown), especially in central and eastern Germany and along the Bavarian Alps.

3.3 Nowcast

Convective cells developing on this day were propagating with the front to the North-East. The cell speed was relatively fast with a median of 70 km/h (Fig. 4), which is typical for the synoptic pattern Cyclonic Westerly (Wapler and James, accepted). With faster moving cells stronger wind gusts are expected. Cell sizes (areas with more than 46 dBZ reflectivity) had typical values, however, cells less frequently reached 54 dBZ reflectivity. Intense cells (with more than 54 dBZ reflectivity) were smaller compared to 6 year cell statistics indicating less chance of hail. Several mesocyclones were detected by radar which correspond well to the above mentioned SDI signal in the COSMO-DE-EPS simulations.

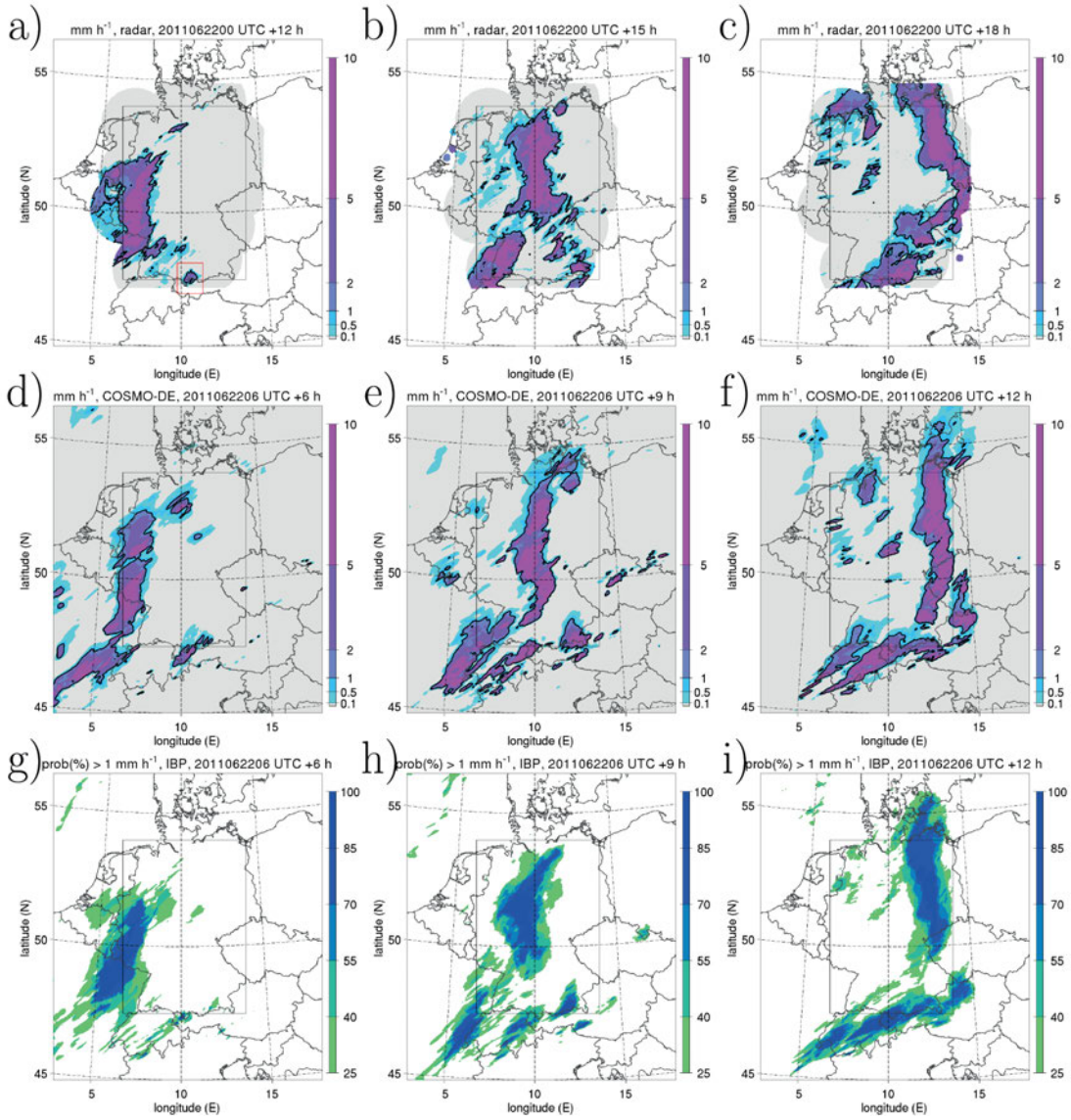

Figure 2: Strong forcing case. Accumulated 1-hourly precipitation of (a–c) radar observations and (d–f) COSMO-DE deterministic forecasts. Thick black contour line shows values larger than 1 mm h^{-1}. (g–i) Ensemble probability forecasts for 1-hourly precipitation larger than 1 mm h^{-1} of COSMO-DE-EPS. Precipitation maps are valid at (a,d,g) 12:00 UTC, (b,e,h) 15:00 UTC and (c,f,i) 18.00 UTC on 22 June 2011. Black solid rectangle indicates Germany domain used for averaging the results. Red solid rectangle in (a) denotes the convective cell which is examined in detail.

Most convective acitivity was associated with the front. However, some pre-frontal convection occurred. One especially strong cell moving along the Bavarian Alps (see red rectangle in Fig. 2a) is described in more detail. This cell caused the highest relative loss.

The temporal evolution of the satellite-based cloud-top cooling rate and the size of the corresponding KONRAD cells is shown in Fig. 5b. The earliest starting point of the satellite-based tracking is at 10:45 UTC around 40 min before the initiation of the radar-based track. At the forward flank of a north-eastward moving cloud field, initiation of deep convection takes place after the crossing of the Alps. A primary cell which develops first has cloud-top temperatures of −15 °C at the beginning and then cools down to −55 °C in the following 70 min. The maximum cloud-top cooling rate is around 18 °C/15 min, reached about 35 min to 40 min before the end of the growth phase. The first KONRAD cell reached the detection threshold of 15 km^2 with more than 46 dBZ at 11:25 UTC. It propagated in east-north-eastern direction with an average cell speed of 57 km/h, one of the slower cells of this day, however fast moving compared to multi-year average cell speeds. As shown in Fig 5b, the primary cell reaches a local maximum in its radar-derived cell size about 80 min after the maximum in cloud-top cooling rate.

Close to 12:00 UTC, a secondary cell develops at the right flank of the primary cell. The secondary cell is obscured by its predecessor; the reason why its cloud-top temperature is only −47 °C at its first detection from satellite. Nevertheless, within a very short cooling duration of 15 min, the cloud-top temperature decreases

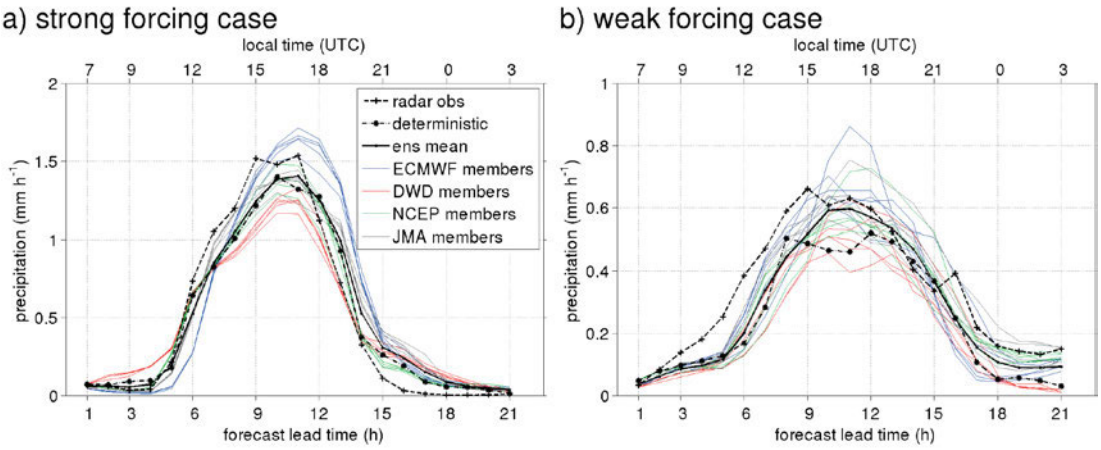

Figure 3: 1-hourly precipitation (mm h^{-1}) averaged over Germany (see black rectangle in Fig. 2): radar observations (black, dashed line), COSMO-DE deterministic (black, dash-dotted line) and COSMO-DE-EPS ensemble mean (black, solid line) forecasts. COSMO-DE-EPS members (colored, solid lines) are shown separated corresponding to their initial and lateral boundary conditions. Results are for (a) the strong forcing case on 22 June 2011 and (b) the weak forcing case on 06 June 2011.

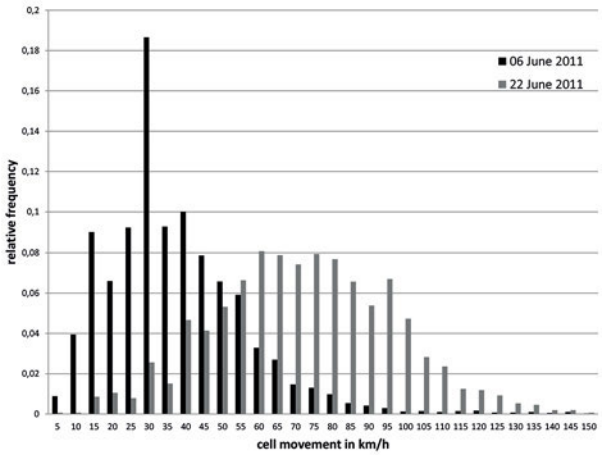

Figure 4: Speed of cell movement for 22 June 2011 (grey) and 6 June 2011 (black). The values are normalised by the total number of cells per day.

down to −62 °C. The rapid cooling and the large and steady anvil edge velocities of about 8 m/s are clear signatures of the development of a severe storm. Three snapshots of the temporal development of the secondary cell are shown in Fig. 6d–f where visible reflectance and infrared brightness temperature from satellite and radar reflectivity factor are combined. A cold-U structure identified in the cloud-top temperatures (Fig. 6e) starts to arise at at 13:10 UTC with a minimum around 210 K probably collocated with the convective core, two cold branches extending downstream of the core and an embedded warm area in between. This strucure is often associated with severe weather phenomena (Adler et al., 1985; McCann, 1983). The cloud-top temperature difference between the coldest parts within the major updraft and the embedded warm area is about 6 K. During the development of the cold-U structure, largest radar reflectivities of about 60 dBZ and highest lightning densities are found in proximity to the minimum cloud-top temperatures. Another indication of the strong updraft is the decrease in the cloud ice effective radius at cloud top from 30 µm at 11:30 UTC to 14 µm at 13:10 UTC. Meanwhile the cloud optical thickness increased from 70 at 11:30 UTC to 150 at 12:15 UTC. The decreasing effective radius combined with an increase in cloud optical thickness is a typical signal for cell intensification and further electrification (Horvath et al., 2012). While only a low number of strokes was measured in the first hour, the lightning activity started to intensify at approximately 12:30 UTC.

Several lightning jumps occurred. The first was measured between 12:30 and 12:50 UTC, with an increase from 25/(5 min) to 224/(5 min), thus a multiplication by a faction of 10 within only 20 min. A second lightning jump occurred between 13:20 and 13:35 with a multiplication of the stroke number with a factor of 3 within 15 min which is equal to increase by 100 strokes per 5 min. Note that the second lightning jump appeared with a time lag of approximately 10 min after the formation of the cold-U structure. The last strong increase of lightning rate was measured at 14:15 when the number of strokes increased by a factor of 1.5. The first lightning jump occurred approximately 30 min prior to the first hail observation, the second at this time (Fig. 7). Thus in this case the lightning jump shows a predictive skill for the estimation of the further cell development and can be used for the warning of the intensification of the cell. Lightning jumps have been reported to occur prior to severe convective weather in the U.S. (Schultz et al., 2009).

The CG+ fraction (ratio of positive cloud-to-ground lightning strokes to all cloud-to-ground lightning strokes) is relatively large with 40 to 60 %. On average the lightning detection network measures a CG+ fraction of 35 %. Lang and Rutledge (2002) found a possible relationship between storm severity and predominantly positive cloud-to-ground activity, however this could not be supported by Hohl and Rutledge (2000).

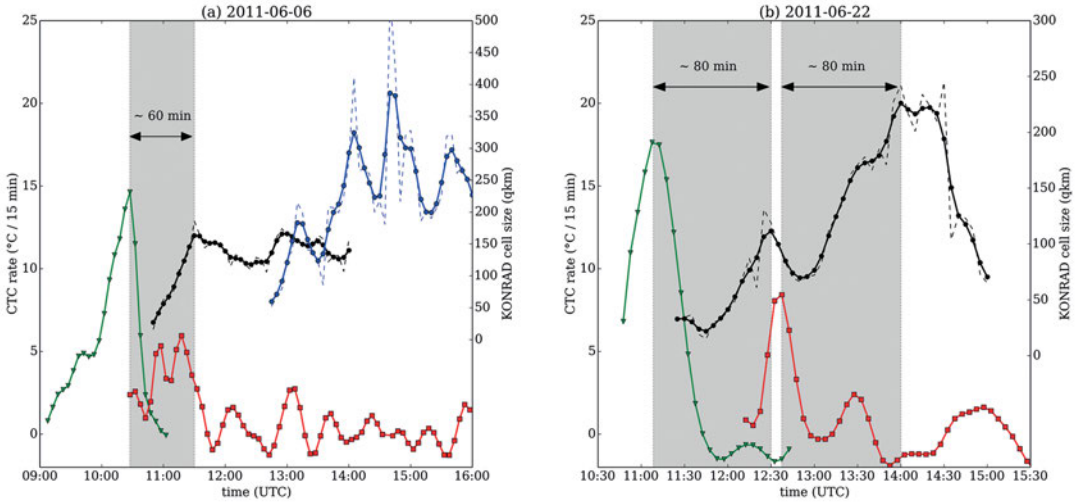

Figure 5: Temporal evolution of satellite-based cloud-top cooling rates (left axis) and KONRAD cell size (right axis) for (a) 6 June 2011 and (b) 22 June 2011. The vertical growth of the primary cell (green) and secondary cell (red) is separately tracked in satellite images. The original time series of KONRAD cell size (thin dashed lines) are smoothed with a Gaussian filter of 5 min width (thick solid lines). Two distinct KONRAD cells (black and blue lines) are detected at 6 June 2011. The time interval between the maxima in cloud-top cooling and KONRAD cell size is highlighted by grey shadings when attribution was possible.

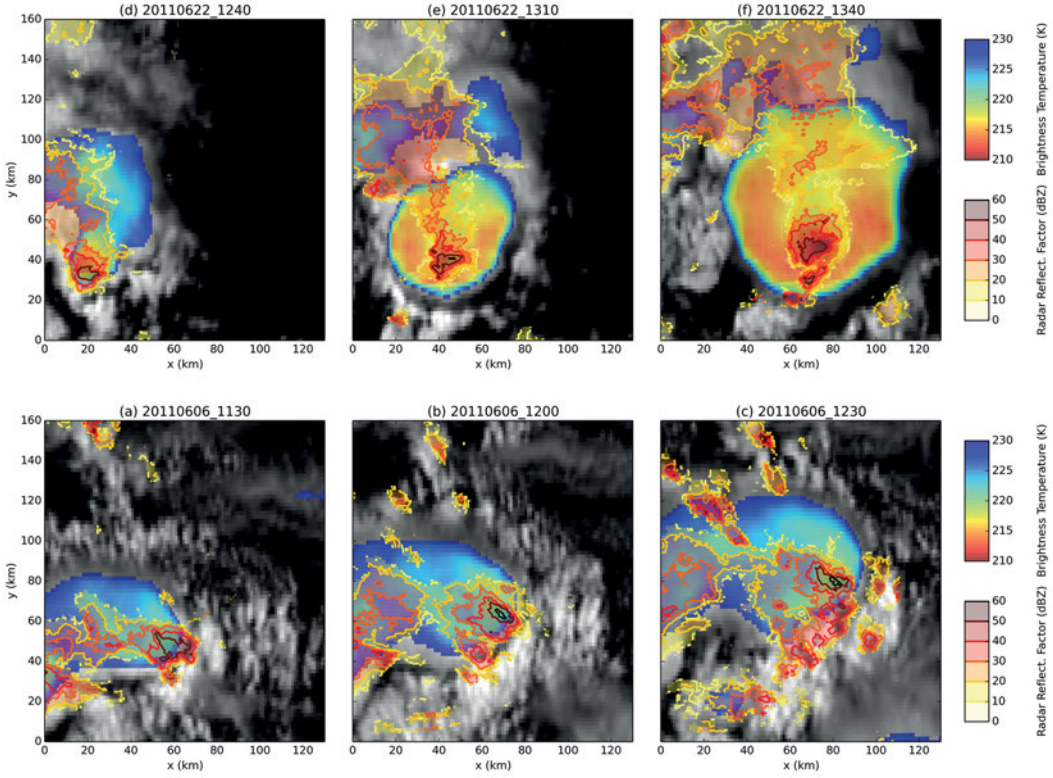

Figure 6: Satellite brightness temperatures and radar reflectivites for 6 June 2011 at (a) 11:30 UTC, (b) 12:00 UTC, (c) 12:30 UTC, and for 22 June 2011 at (d) 12:40 UTC, (e) 13:10 UTC and (f) 13:40 UTC. High-resolution visible reflectivities (grey shades) are overlaid by infrared brightness temperatures (colors) for which only values colder than 220 K are shown with decreasing temperature from blue to red. The colored contour lines show radar reflectivity.

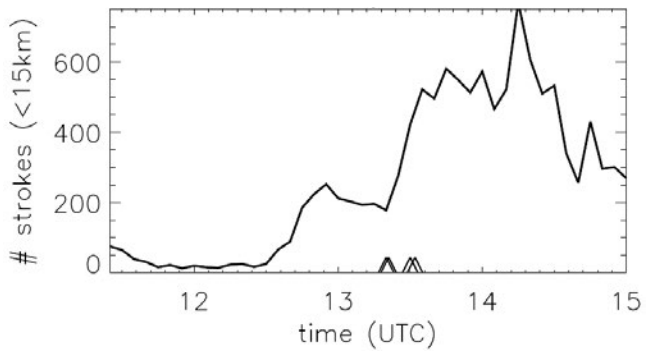

Figure 7: Temporal evolution of lightning rate on 22 June 2011 between 11:30 and 15:00 UTC. The triangles indicate the time of the ESWD hail reports.

The cell also shows high values of vertically integrated liquid (VIL) which is a clear signal for hail. The maximum value of 46 l/m^2 was reached at 13:15 and at 14:00 UTC.

3.4 Warning

Warnings valid from 14:00 to 15:00 UTC on 22 June are shown in Fig. 8 (c, d) and compared to ESWD reports and lightning observations. Considering the warning category mainly "strong thunderstorm" warnings and for some regions "thunderstorm with hail" were issued. Most districts for which lightning activity has been observed and most areas in which severe weather has been reported are appropriately warned. Only few lightning events downstream of the frontal line are not covered by warnings (misses) while large areas upstream are warned with, however, no lightning activity observed (false alarms). Considering the lead time for that hour of issued warnings it is generally found, that downstream the warnings are issued at most 1 hour in advance, in many cases not until the time when lightning activity has already been observed. Upstream of the front, lead times are larger with warnings issued 1 or 2 hours in advance, likely to be related to the too slow propagation predicted in the short range forecasts (compare Section 3.2). Consistently, the districts affected by the severe hailstorm related to the strong cell moving along the Bavarian Alps have been appropriately warned with the highest category ("Thunderstorm with hail"), however warnings were basically issued at the hour when hail has occurred. Basic verification results of thunderstorm warnings against lightning observations are shown in Fig. 9b. The number of districts in which lightning occurred increased during 22 June reaching maximum affectedness of 134 out of 413 districts between 14:00 and 15:00 UTC. Most of these lightning events are covered by the issued warnings (indicated by the number of hits being close to the number of events) and rather few missed events. The number of false alarms raises to about 50 to 70 districts per hour in the late afternoon, which as mentioned above is due to the warnings being valid too long leading to an overwarning upstream of the front. During the course of the day 910 "events" were observed in total, with 765 being correctly warned, 145 being missed and 713 false alarms. This corresponds to a Probability Of Detection (POD) of 0.84, a Missed Event Rate (MER) of 0.16 and a False Alarm Ratio (FAR) of 0.48.

3.5 Weather impact and damage

Three tornado events are found in the ESWD (Fig. 10b). One was observed near Altenlotheim (Hesse, 51.129/ 8.917) at 13:09 UTC. More than two hours later (at 15:44 and 15:47 UTC) tornadoes were observed near Dölzig (Saxony, 51.35 ° N/12.217 ° E) and Gröbers (Saxony-Anhalt, 51.44 ° N/12.12 ° E). All events are classified as F1/T3 and have a path length of up to 4 km.

Several hail observations are collected in the ESWD, especially along the Northern Edge of the Alps in Southeast Germany. The maximal thickness of a hail layer of 4 cm was observed near Bad Tölz (Bavaria, 47.761 ° N/11.559 ° E) at 13:20 UTC. The maximal hail size of 3.5 cm was recorded in Waschbrunn (Bavaria, 47.862 ° N/12.055 ° E) at 13:32 UTC.

The 140 ESWD wind reports are recorded between 14:00 and 18:00 UTC mainly in the central and eastern parts of Germany. 17 synop stations measured gusts with more than 90 km h^{-1}, 5 of them even recorded more than 100 km h^{-1} (see Table 1).

Rain rates of more than 15 mm h^{-1} were recorded at 122 out of 1205 rain gauge stations and 11 stations exceeded 25 mm h^{-1}. The maximum rain rate of 35.4 mm h^{-1} was observed at the station Rheinfelden (Baden-Württemberg, 47.564 ° N/7.794 ° E). Accumulated daily rainfall exceeded 30 mm d^{-1} at 26 measurement stations with a maximum rainfall of 46.4 mm d^{-1} at the stations Rheinfelden and Enkenbach (Rheinland Pfalz, 49.530 ° N/7.889 ° E).

The total amount of losses on 22 June accounted for 53.9 Mio EUR corresponding to a German-wide loss ratio of 0.0076. In the period of 1997–2011, only 17 days in summer (neglecting widespread damages caused by winter storm events) feature higher loss ratios. Considering the spatial distribution of occurred losses, good agreement with the ESWD severe weather reports is found (Fig. 10b). High loss ratios are found in the Eastern parts of Germany which have been affected by severe winds. In Southern Germany, two bands featuring high losses can be identified. The first is related to the severe thunderstorm cell described above traveling along the edge of the Alps affecting districts at the border to Switzerland and Austria with highest losses in the Bavarian districts Bad-Tölz, Miesbach, Bad-Aibling and Weilheim-Schongau. Within the period 1997–2007 for which loss records are available, only one summer event (2 August 2001) has been recorded that leads to higher losses in these districts. The second band is found about

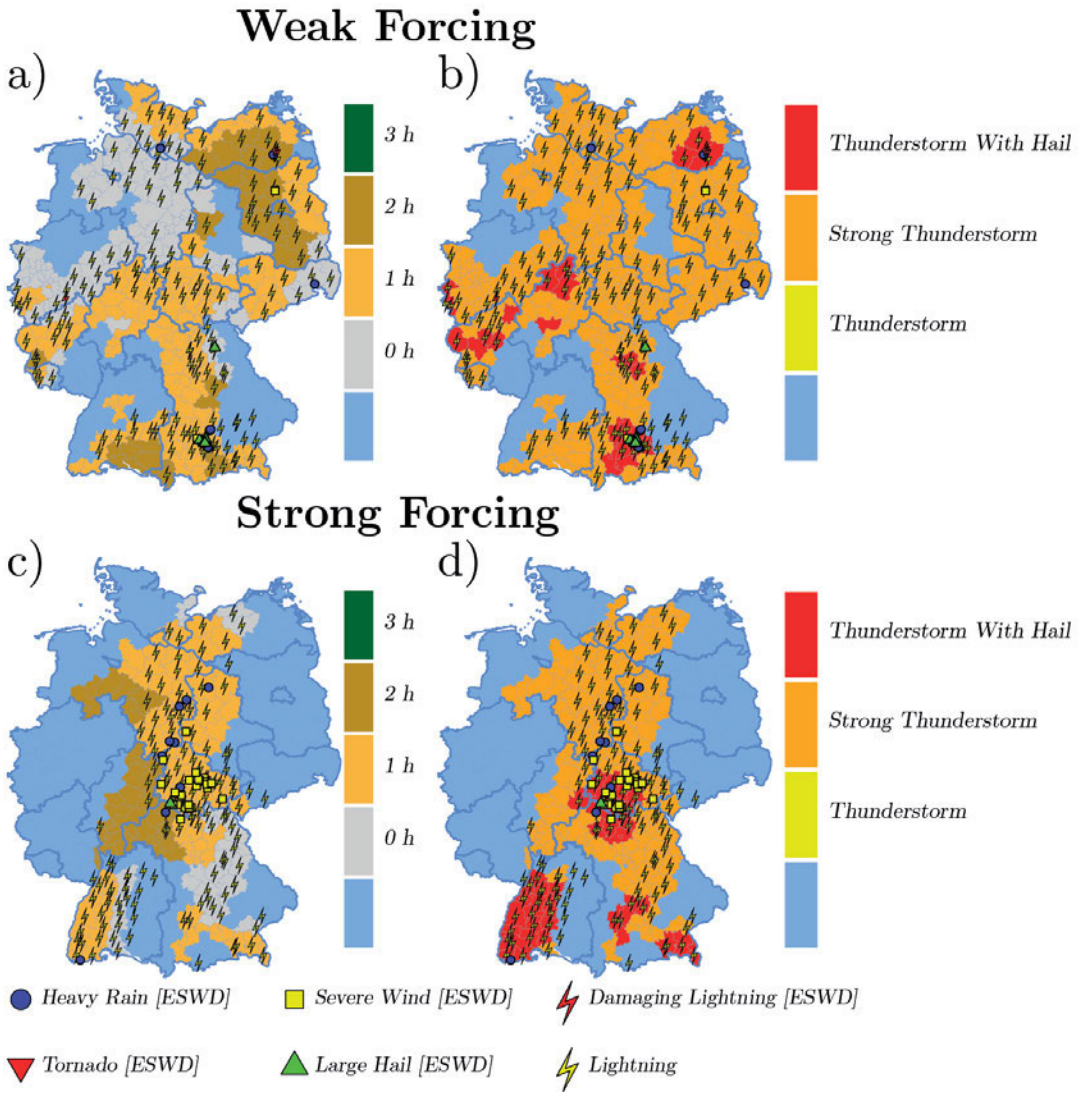

Figure 8: Comparison of issued warnings on district level and severe weather observations. (a,b) Weak forcing case 6 June 2011: Warnings issued for the hour 14:00–15:00 UTC. (c,d) Strong forcing case 22 June 2011: Warnings issued for the hour 14:00–15:00 UTC. (a) and (c) show lead times of the issued warnings in hours, (b) and (d) show the issued warning categories respectively. Data sources: German Weather Service, European Severe Weather Database, GeoBasis-DE / BKG 2013.

100 km to the north stretching from the western border of Germany towards central Bavaria. Slightly lower losses are found with only few related ESWD reports.

4 The weak forcing case: 6 June 2011

4.1 Synoptic overview

On 6 June 2011 an amplifying upper level trough laid off the continental European west coast (Fig. 11). In Germany a weak southwesterly upper flow existed. A weakening small upper low was embedded in this flow and migrated from N Italy into the Czech Republic/S Poland. Warm moist air was present over central Europe with weak to moderate potential instability. The synoptic pattern is classified as Sz (Cyclonic Southerly) according to James (2007). Dynamic large-scale lifting was missing, thus convection was triggered mainly thermally and orographically. The area averaged convective adjustment time scale reaches peak values of more than 12 h around 12:00 UTC which classifies this day as weak forcing case (Zimmer et al., 2011). The 6 June 2011 was characterized by widespread, localized precipitation occurring in the afternoon over Germany (Fig. 12). The radar observations show intensive convective development around 12:00 UTC that prevailed throughout the afternoon (Fig. 12a–c). Several small convective precipitation events and some few larger and more intense regions of precipitation are found over central Germany and also in the South close to the Alps.

The (human) forecast issued on 1 June 2011 predicted that thunderstorms with heavy rain, strong gusts and hail are possible on 6 June 2011 for whole Germany and locally possibly severe.

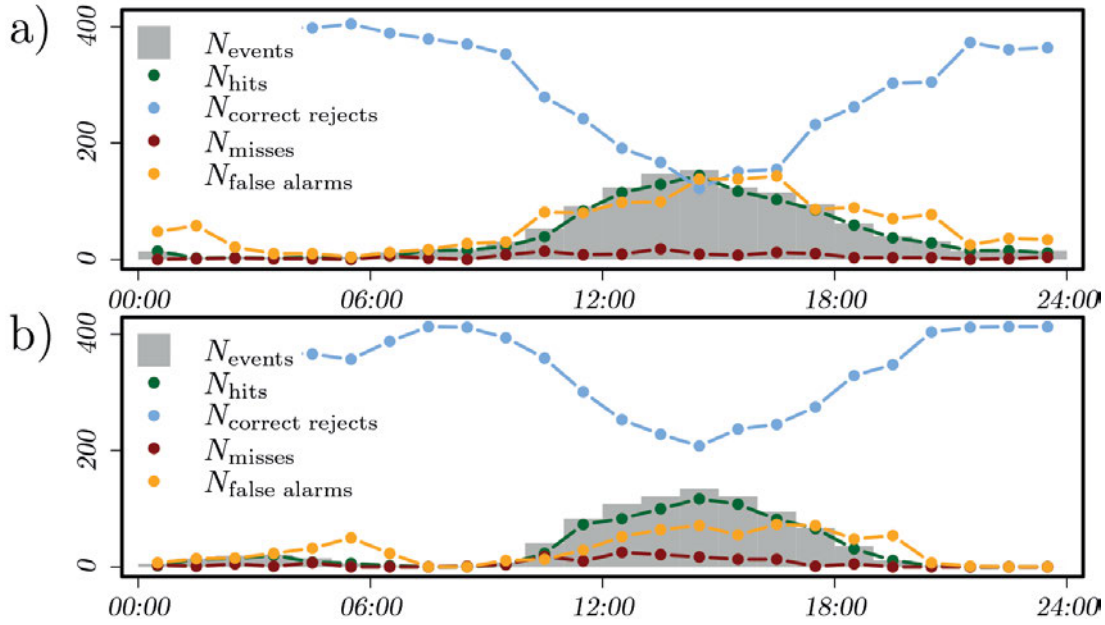

Figure 9: Basic verification of issued thunderstorm warnings against lightning observations on (a) 6 June and (b) 22 June 2011. The number of districts in which lightning occurred (N_{events}) are shown in grey bars. Number of hits (lightning event and warning issued), misses (lightning occurred and no warning issued), false alarms (lightning did not occur but a warning was issued) and correct rejects (no lightning and no warning) are shown in colors.

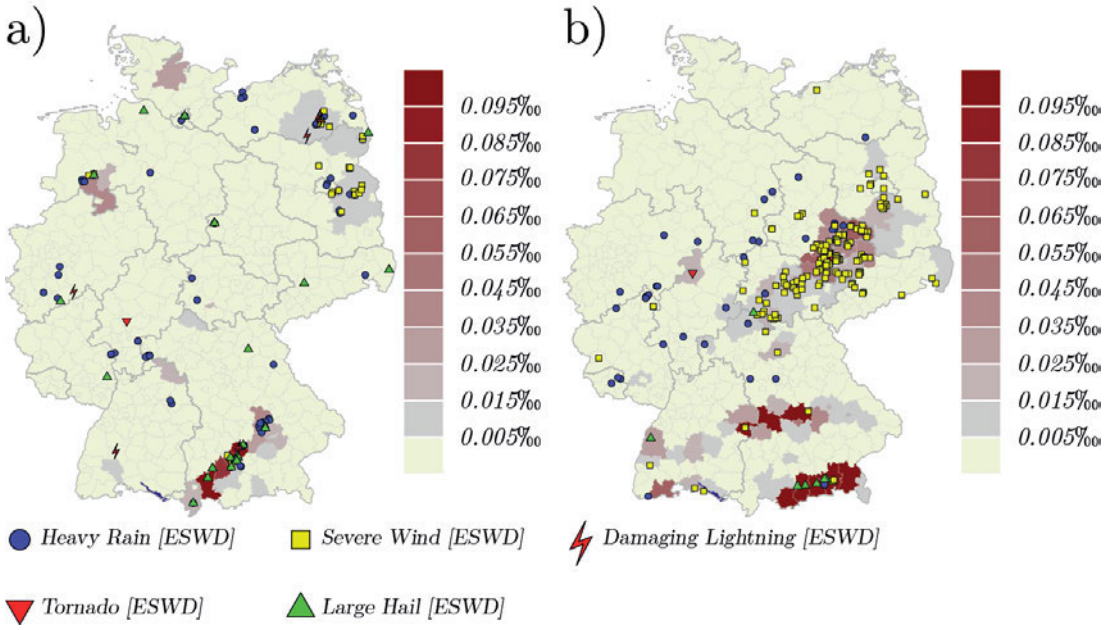

Figure 10: Loss ratio (per thousand) on district basis for (a) 6 June 2011 and (b) 22 June 2011 in comparison to the occurred severe weather reports from the ESWD. Data sources: Gesamtverband der Deutschen Versicherungswirtschaft e.V., European Severe Weather Database, GeoBasis-DE/BKG 2013.

4.2 Short-range forecast

The deterministic and ensemble forecasts of precipitation give a scattered distribution of convective precipitation regions over Germany during the day (Fig. 12). This highlights that the model predicts correctly the patchy precipitation structure of the day, but it is clear that the timing and location of the precipitation is not exact and often does not agree very well with the radar observed location. During weak-forcing, the forecasts are strongly affected by both the lower predictability of the single convective cells itself and the model uncertainty. Probability forecasts of the COSMO-DE-EPS show scattered regions with relative high probabilities which again points to a likely under dispersiveness of the ensemble forecasts.

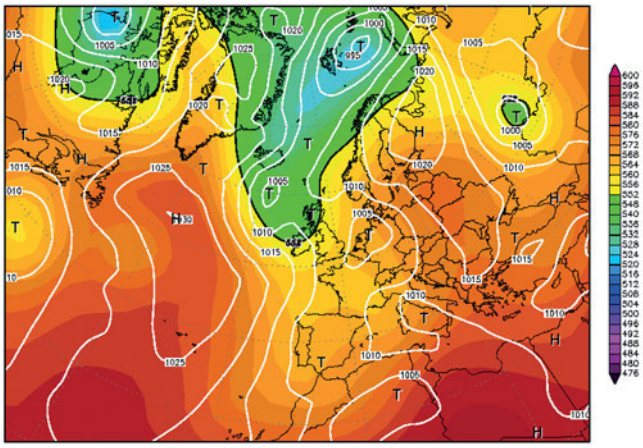

Figure 11: 500 hPa geopotential and surface pressure on 00:00 UTC 6 June 2011. Taken from www.wetterzentrale.de.

During the weak-forcing day all ensemble members have problems to correctly forecast the onset of the convection and the domain averaged precipitation over Germany shows an underestimation of the precipitation until the afternoon hours around 15:00 UTC (Fig. 3b). At the period of peak precipitation between 15:00–18:00 UTC the predicted amounts agree with the observed ones. The ensemble mean still underestimates the precipitation, but a number of ensemble members predict equal or larger amounts than observed. The decay in precipitation activity towards the night is captured correctly in the deterministic and ensemble forecasts. In the absence of a synoptic large-scale forcing, the ensemble members with different driving global models show similar results and no clear separation of the members with respect to their driving model is found.

4.3 Nowcast

Most cells of the day were moving with a speed of about 30 km/h (Fig. 4) in northern directions. As typical for the synoptic pattern Sz, a high fraction of KONRAD cells exhibits a hail warning flag. Parts of the north to northwestward moving fields of low- to mid-level cumulus clouds can already be attributed to the later deep convective complex at 9:00 UTC.

A supercell in Bavaria, which caused the highest losses, is described in more detail and the temporal evolution of its cloud-top cooling rate and KONRAD cell size is given in Fig. 5a. In the manual backtracking, the starting point of the track is next to the southern Austrian border. However, the initiation of deep convection occurs roughly two hours later after crossing the Alpine ridges. A multicellular complex develops in the following with newly initiated secondary cells appearing on its right flank. Cloud-top temperatures of around −5 °C at the beginning of the tracking slowly decrease to around −50 °C at the time of the storm cell's mature phase. Minimum cloud-top temperatures of −58 °C are observed in subsequently developing updraft cores. The maximum cloud-top cooling rate of around 16 °C/15 min is reached around 35 min to 40 min before the end of the growing phase as reported for a set of similar cases in Senf et al. (accepted). The time lag between the maximum in cloud-top cooling of the primary cell and the first maximum KONRAD cell size is around 60 min. The sequential evolution of a secondary cell from 11:30 to 12:30 UTC is shown in Fig. 6a-c. The maximum in radar reflectivity of 68 dBZ is nearly colocated with the minimum of cloud-top temperature.

The equivalent diameter of the corresponding cirrus anvil changes from around 10 km at 10:00 UTC to 40 km at 11:00 UTC reaching finally 70 km at 12:30 UTC (not shown). The average anvil edge velocity which is a measure of the strength of the anvil expansion slowly decreases in the first two hours from 6 m/s to 2 m/s.

A mesocyclone was identified in radar images at 11:30 (not shown). The cell intesified while moving to the NE. Following a phase of continuous growth of the lightning rate, a lightning jump (increase of a factor of 5 within 10 minutes) occurred at 13:00 UTC. At this time hail layers of 10 cm thickness were found on the ground. The highest lightning stroke rate reached more than 550 strokes per 5 minutes. The cell also shows high values of vertically integrated liquid (VIL) clearly indicating hail. The VIL first reached values above 40 l/m^2 at 12:10 UTC. The maximum value of 50 l/m^2 was reached at 12:35.

4.4 Warning

Issued warnings appropriately covered most of the observed thunderstorm events, according to lightning observations (Fig. 8). Also severe weather events were adequately indicated by the warnings. A rather strong overwarning can be noticed. The cells in Bavaria featuring severe hailstorms have also been adequately captured by the warnings that were issued. For most of the "large hail" reports, warnings have even been issued 1 or 2 hours in advance. Around 16:00–17:00 UTC, the cells weakened while moving north-eastward. However, warnings with the highest category ("Thunderstorm with hail") were issued for large parts of eastern Bavaria until 19:00 UTC indicating that the weakening of the supercell was not correctly captured. Verification of thunderstorm warnings as shown in Fig. 9a exhibits that most of the lightning events are appropriately covered by the issued warnings with very few of the events being missed. However strong overwarning can be diagnosed and the number of false alarms is in the same order of (or even exceeding) the number of events observed. Warnings have been issued for an area about two times larger than the area where lightning has been observed (Fig. 9a). In total, during 6 June 1190 events have been observed, with 1068 hits and 122 misses. However, the total number of 1431 false alarms is found to be exceptionally high, with a False Alarm Ratio (FAR) of 0.57.

4.5 Weather impact and damage

Weather impacts on 6 June 2011 are scattered across Germany with various "large hail" as well as "heavy

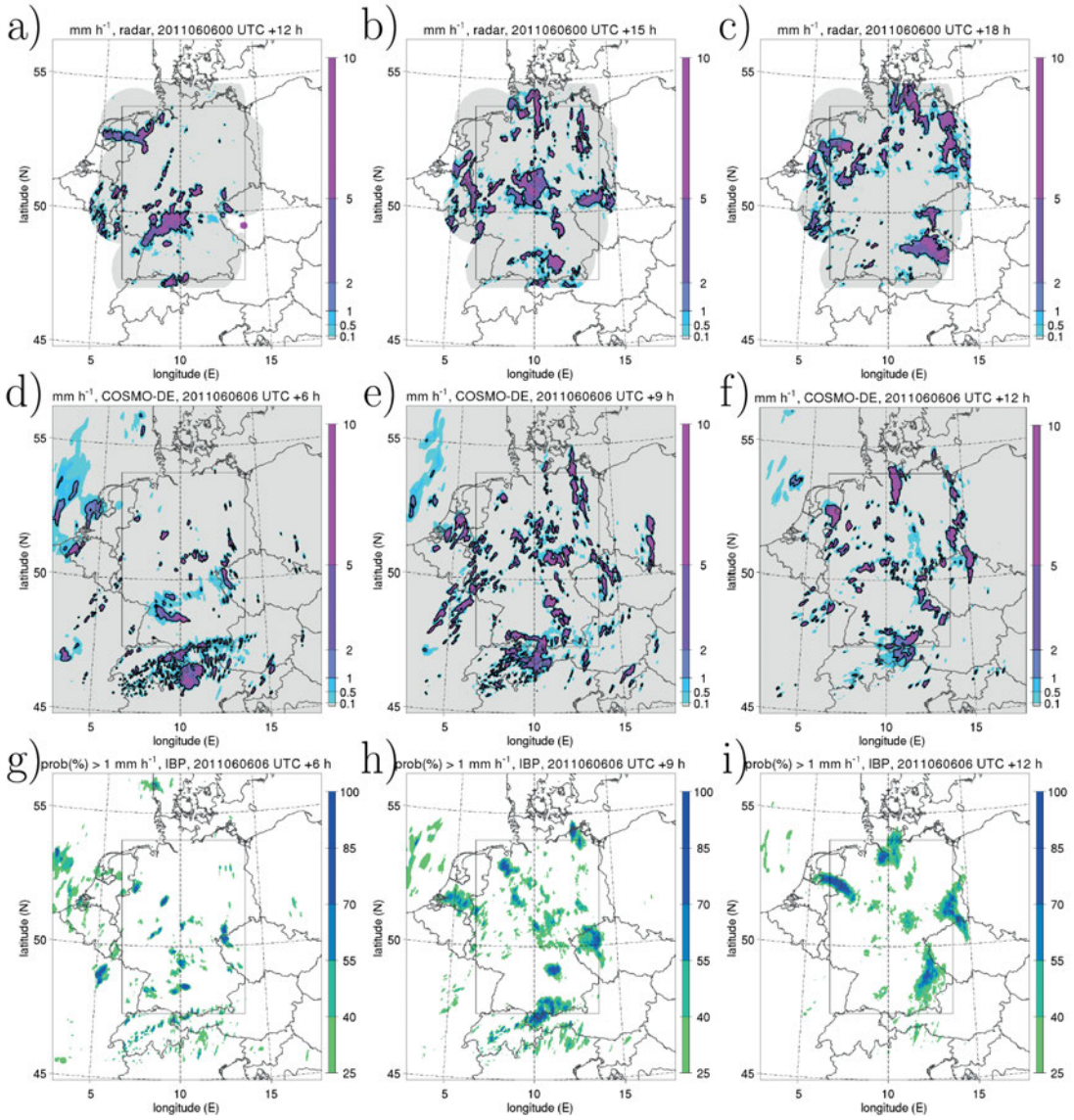

Figure 12: Weak forcing case. Accumulated 1-hourly precipitation of (a–c) radar observations and (d–f) COSMO-DE deterministic forecasts. Thick black contour line shows values larger than 1 mm h^{-1}. (g–i) Ensemble probability forecasts for 1-hourly precipitation larger than 1 mm h^{-1} of COSMO-DE-EPS. Precipitation maps are valid at (a,d,g) 12:00 UTC, (b,e,h) 15:00 UTC and (c,f,i) 18:00 UTC on 06 June 2011. Black solid rectangle indicates Germany domain used for averaging the results.

rain" observations reported in the ESWD database (see Table 1 and Fig. 10). Also in North-East Germany (Brandenburg and Mecklenburg-Vorpommern) reports on "severe wind" and "damaging lightning" have been recorded. The occurred losses scatter across Germany, however agreement with ESWD reports is weak. In Brandenburg and Mecklenburg-Vorpommern severe weather reports coincide with districts featuring moderate losses. The supercell in the south of Bavaria, emerging at the edge of the Alps in the southwest and travelling towards north east, can be identified by multiple "large hail" and "damaging lightning" observations from the ESWD data base. Furthermore, analysis of insured losses shows high losses on a narrow band in this area. While there are districts with no ESWD report, damage data show that severe weather conditions leading to high impacts have occurred continuously on the cell's path. The synopsis of observational data and insured losses thus gives insight on the characteristics of the local severe weather conditions, combining information on their spatial extent as well as their meteorological properties.

In total, losses on 6 June accounted for 24.5 Mio EUR, with the largest share of losses occurring in the regions affected by the cell described above. In some of these districts loss ratios feature the highest losses within the period of data availability (1997–2007).

The largest hail stones have a maximum diameter of 7.2 cm, occurring at 14:17 UTC in Gernlinden-Ost (Bavaria, 48.23 ° N/11.31 ° E). Hail layers with a maximum thickness of 10 cm are recorded for Kauf-

beuren (Bavaria, 12:35 UTC, 47.883 ° N/10.617 ° E) and Buchloe (Bavaria, 13:00 UTC, 48.033 ° N/ 10.733 ° E). The thickest hail layer of that day measures 20 cm and is recorded near Ansbach (Bavaria, 48.4 ° N/ 11.45 ° E) at 15:05 UTC.

Furthermore, 18 surface stations measured wind gusts with more than 65 km/h, but no wind gusts above 90 km/h (25 m/s) occurred.

Rain rates larger than 15 mm h^{-1} were recorded at 66 of 1205 rain gauge stations and 19 (3) stations exceeded 25 mm h^{-1} (40 mm h^{-1}). The maximum rain rate of 53.5 mm h^{-1} has been observed at the station Kirchdorf/Poel (Mecklenburg-Vorpommern, 54.001 ° N/11.436 ° E). Accumulated daily rainfall exceeded 30 mm d^{-1} at 34 stations with recordings above 50 mm d^{-1} at 3 stations, the maximum daily rainfall of 71.0 mm d^{-1} again being observed at Kirchdorf/Poel.

5 Comparison and discussion

This section compares the strong forcing (SF) and weak forcing (WF) case and highlights differences as well as similarities.

Using the convective adjustment time-scale as an indicator for the existence of a strong large-scale synoptic forcing, the two cases can be clearly distinguished. The SF case on 22 June 2011 shows convective precipitation events that are mainly triggered by a large-scale synoptic forcing. The WF case on 6 June 2011 is characterised by the absence of a large-scale forcing and convective precipitation is due to local forcing mechanisms and shows a more locally heterogeneous pattern. The WF and SF case exhibit a different spatial precipitation structure (Figs. 2, 12) even though the daily distributions of the average precipitation over Germany (Fig. 3) are qualitatively similar to each other.

The differences in the forcing lead to differences in the early warning information issued 5 days ahead of the events. While thunderstorms were forecasted with higher probabilities in the SF case ('likely') when a synoptic disturbance was expected to affect Germany, in the WF case the probabilities of thunderstorms was lower ('possible').

For the SF case, the ensemble forecasts show high probabilities (≥ 80 %) of intense precipitation moving across Germany (Fig. 2) in the short-range forecasts (< 21 h) and the deterministic and ensemble forecasts are able to give guidance on the location and timing of the precipitation about 6 to 12 h in advance. For the WF case, the model short-range forecasts show a broad region with scattered convective precipitation events over Germany (Fig. 12), but there is considerable uncertainty about the location, timing and intensity. Further, it seems that the probabilities are overforecasted due to not enough spread in the ensemble forecasts. The total amount of precipitation in the afternoon is underestimated even though some ensemble members indicate larger precipitation amounts (Fig. 3b).

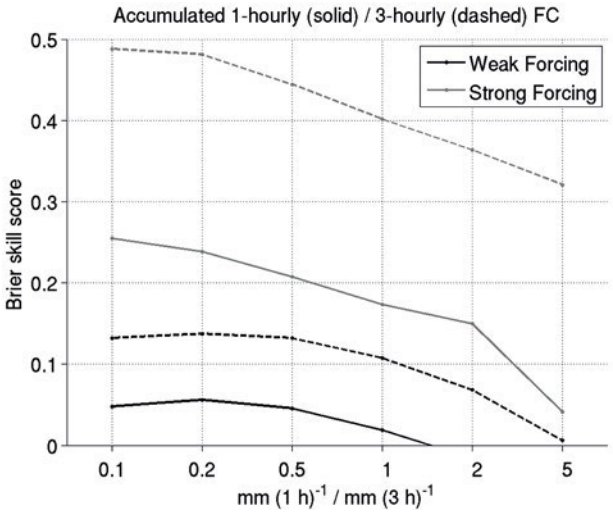

Figure 13: Brier skill score for different thresholds of accumulated 1-hourly (solid) and 3-hourly (dashed) precipitation forecast averaged over 1–21 h forecast lead times in the Germany verification domain.

Comparing this result with the whole summer 2011 (see Fig. 5 in Kühnlein et al. (2014)), the SF case behaves similar to the whole period with slight overestimation of precipitation early in the forecast, a good agreement in the afternoon and a large overestimation of precipitation from 15 h onwards. The WF case show a slightly different behaviour and the precipitation amounts are in better agreement with the observations for this case here. The tendency to underestimate the precipitation in the late afternoon is similar to the whole period.

To assess the skill of the precipitation forecasts for the SF and WF case, the Brier skill score (BSS) has been computed (Wilks, 2011):

$$BSS = \frac{\text{"Resolution"} - \text{"Reliability"}}{\text{"Uncertainty"}}. \qquad (5.1)$$

The uncertainty is defined here from the given set of verifying observations. The forecasts are skillfull if the BSS is between 0 and 1, with 1 being the best. Verification is done against radar observed precipitation for in the Germany verification domain (Figs. 2,12) and observational errors are neglected here. The BSS is calculated for different thresholds of accumulated 1-hourly and 3-hourly precipitation: 0.1 mm, 0.5 mm, 1 mm, 2 mm and 5 mm.

The skill is much lower for the WF case compared to the SF case (Fig. 13). Especially, for accumulated 1-hourly precipitation forecasts the skill is very low and for larger thresholds above 2 mm h^{-1} the COSMO-DE-EPS forecasts do not have any skill at all. This confirms that in the absence of a large-scale trigger mechanism precipitation forecasts on the grid scale for short time intervals are very difficult and for the WF case there is no skill in the forecast of single intense convective cells. However, if one relaxes the time constraint and consideres longer time intervals, the skill can be improved for

accumulated 3-hourly precipitation forecasts. In the SF case, where the cold front mainly determines the precipitation, the COSMO-DE-EPS forecasts have skill for accumulated 1-hourly and 3-hourly forecasts among all considered thresholds. The skill can also be significantly increased for the SF case by extending the considered time interval.

The differences in skill on SF and WF cases agree with other case studies using the convective adjustment time-scale τ_c and the normalized ensemble spread to charaterise the corresponding predictability on different days (Keil et al., 2014). Larger values of the convective adjustment time-scale τ_c are connected with larger ensemble spread which indicates less predictable situations and leads to a lower skill in the forecasts for the WF case.

The different forecast skill of both case studies is in accordance with the seasonal investigation of Keil et al. (2014). SF and WF weather regimes exhibit different levels of predictability and forecast skill. During WF both the predictability, as measured with the normalized ensemble spread, and the forecast skill are lower assessed with deterministic and probabilistic measures.

The direction of cell movement shows a narrow distribution in the SF case, where cells move with the strong background flow. In contrast, the cells in the WF case have a wider direction distribution which might be related to weaker background flow. As shown in Fig. 4, the cells in the SF case moved much faster, thus producing stronger gusts. In contrast the cells in the WF case are associated with weaker gusts, but with a higher fraction of hail. This is also reflected in the VIL values which are higher in the WF case.

The characteristics of the most intense thunderstorm cells did not show significant systematic differences between the WF and the SF case. In both cases typical life cycles of individual cells can be derived from various sensors. At the beginning, the cells are best visible in satellite images and rapid cloud top cooling hints at strong convective cell development. Furthermore, changes in the satellite-observed cloud anvil size give information on the updraft strength and possible further cell intensification and lifetime. Once the cell is detectable in radar observations, cell sizes and vertical characteristics such as VIL show the intensity of the cells. Additional insights in the potential of the later severity are obtained by lightning rates, as evident for lightning jumps, and features in stellite imagery, as cold-U-shaped cloud-top temperatures and pronounced overshooting tops in the severe Bavarian cell in the SF case.

Overall the issued warnings adequately covered the reported severe weather events for both the WF as well as the SF case. In the SF case, some thunderstorm events are missed downstream of the front or else warnings being issued only very shortly in advance. Upstream of the front, warnings are issued further in advance, but an overwarning can be noticed as issued warnings are valid too long which is likely related to a too slow propagation predicted. Thus, monitoring and correcting propagation forecast errors can improve the timing of warning in situations with fast moving precipitation systems. The severe thunderstorm cells occurring at the front are well captured in their intensity. Correct warnings have been given, however, with short to zero lead time. In comparison in the WF situation a stronger overwarning is observed in connection to longer lead times of issued warnings. The supercell that occurred in Bavaria in the WF case has been accordingly captured by the warnings with generally higher lead times compared to the cells in the SF case. Noticeable in this case is the missed weakening of the cell while it is moving north-east which leads to a strong overwarning in eastern parts of Bavaria consistent with the general overwarning observed in the WF case. This may be improved if more information on the convective life cycle should be included in the nowcasting and warning process. The verification of issued warnings revealed that in both cases most thunderstorm events were adequately warned, with only few events being missed. However in the WF case, a strong spatial overwarning is observed with warnings issued for about twice the area in which lightning actually occurred. This overwarning is generally found to be lower in the SF case, in terms of the FAR being 0.48 compared to a FAR of 0.57 in the WF case.

In the WF case weather impacts were dominated by hail and severe precipitation. At multiple observation stations, precipitation rates as well as accumulated daily rainfall exceeded thresholds defining severe weather conditions according to the DWD ($25\,\mathrm{mm\,h^{-1}}$/$50\,\mathrm{mm\,d^{-1}}$). Severe weather reports included an observation of hail with a diameter of 7.2 cm. In the SF case, precipitation rates and accumulated rainfall were lower compared to the WF case, with fewer observations fullfilling severe weather criteria and a maximum observed hail diameter of 3.5 cm. In the SF case however, widespread areas were affected by severe winds with maximum gusts exceeding $100\,\mathrm{km\,h^{-1}}$ in some regions (see Table 1 and Fig. 10). In terms of impacts, both situations have led to considerable losses, in both cases multiple thunderstorm cells occurred which led to immense losses locally.

The two cases were also quite exceptionally in terms of requests for weather and weather warning information via the World Wide Web. Based on the web traffic on DWD's web sites for the summers 2008–2013 the Monday 6 June 2011 (Wednesday 22 June 2011) represented the 99 % (97 %) quantile of page impressions on http://www.dwd.de and the 85 % (96 %) quantile on the dedicated warning web site http://www.wettergefahren.de.

6 Summary

A strong and a weak forcing severe convective day are analysed in detail using a multi-data approach. Various data sources, including in-situ and remote sensing observations, damage reports and insurance data, information

access by the public, nowcasting algorithms and high-resolution model forecasts are analysed. It is shown that the different data complement one another to provide a more comprehensive characterisation of the events. For example using both loss data from insurance data and eye witness reports from the ESWD enables a better assessment of the impacts. While the loss data provide spatially continuous information, the ESWD provide point observations with more meteorological details of the impact. Further, precise ground wind measurements and station measurement data only available at a limited number of observation points can be complemented by loss data to provide a spatially complete depiction. Thus, using data from various sources allows to combine the different strengths of observational data sets, especially in terms of spatial coverage and data accuracy. Most data either provide good spatial coverage but low precision due to indirect observations, e.g. the exact wind speed can hardly be derived from loss data. Other data sets have a high physical precision, as is the case of direct wind measurements, but provide information for only few points.

Analysing the issued warnings, it is found that in both cases district warnings are issued with very short lead times which are slightly longer in the strong forcing case. Standard practice in operational warning of convective events is to 'warn on observation' (Stensrud et al., 2009) which typically leads to these very short lead times. However, this might be mitigated with advanced consideration of the life cycle of convective events in nowcasting algorithms and thus the warning process. This could lead to earlier warnings providing a longer lead time to prepare for the event.

By shifting to a probabilistic view, even longer lead times are possible using high-resolution EPS systems which provide a new guidance for the forecaster well before the convection even started. They might turn this information into a watch for the users to get prepared for possible severe weather warning. The benefit of probabilistic information based on an EPS system compared to deterministic forecast is that the probabilistic information enables the forecaster to mitigate the problem to be either precise or timely. The EPS can provide different possible forecast scenarios instead of just one realisation for the deterministic case. However, if applying the forecasts for warnings the different predictability situations of the atmosphere have to be considered with lower predictability in WF cases and higher predictability in SF cases. In case of low predictability, also the skill of the forecast is expected to be relatively low.

Due to uncertainty in the location as well as in the temporal evolution of the convective events, an overwarning occurs spatially, in terms of the size of the warning area, and temporally, in terms of the duration of the warning.

This overwarning occurs for both cases but is stronger in the WF case. This is due to the fact that in the SF case the region with convective activity is rather well defined by the knowledge about the location of the frontal line, which is not the case in the WF case. However, the knowledge about the timing (evolution) of single convective cells is limited in both cases. To be overcautious, warnings are thus usually issued with a rather long duration. In both cases this leads to a typical overwarning after the peak of thunderstorm activity. A better understanding of the life cycle could thus reduce the overwarning during the weakening phase of convective events. Some parameters that show predictive skill for convective development are shown exemplary in the present study: e.g. satellite derived cloud top cooling rates for convective initiation and growth and lightning jumps, overshooting tops and enhanced cloud-top features for the mature phase.

In summary, three main conclusions can be drawn from this study: (a) the combination of various data sources allows a better assessment of the characteristics and impacts of severe weather events and provide a more complete picture of the different stages of the convective life cycles and could thus improve nowcasting and warning, (b) warning and forecast performance differ betweeen the weak and the strong forcing case and (c) the presence of large-scale forcing mechanisms increases the forecast skill of convective events. Although evident for the presented case studies, more robust conclusions might be drawn from an extension of this study to further cases.

Acknowledgements

This research was carried out in the Hans-Ertel-Centre for Weather Research. This research network of Universities, Research Institutes and the Deutscher Wetterdienst is funded by the BMVI (Federal Ministry of Transport and Digital Infrastructures).

References

Adler, R.F., M.J. Markus, D.D. Fenn, 1985: Detection of Severe Midwest Thunderstorms Using Geosynchronous Satellite Data. – Mon. Wea. Rev. **113**, 769–781.

Baldauf, M., A. Seifert, 2008: Forecasting of severe weather with the convection resolving model COSMO-DE. – EGU General Assembly, 13–18 April 2008, Vienna.

Baldauf, M., A. Seifert, J. Förstner, D. Majewski, M. Raschendorfer, T. Reinhardt, 2011: Operational convective-scale numerical weather prediction with the COSMO model: description and sensitivities. – Mon. Wea. Rev. **139**, 3887–3905, DOI: 10.1175/MWR-D-10-05013.1.

Barthlott, C., R. Burton, D. Kirshbaum, K. Hanley, E. Richard, J.-P. Chaboureau, J. Trentmann, B. Kern, H.-S. Bauer, T. Schwitalla, 2011: Initiation of deep convection at marginal instability in an ensemble of mesoscale models: a case-study from cops. – Quart. J. Roy. Meteor. Soc. **137**, 118–136.

Betz, H.D., K. Schmidt, P. Laroche, P. Blanchet, W. Oettinger, E. Defer, Z. Dziewit, J. Konarski, 2009: LINET – An international lightning detection network in Europe. – Atmos. Res. **91**, 564–573.

Cintineo, J., M. Pavolonis, J. Sieglaff, A. Heidinger, 2013: Evolution of severe and nonsevere convection inferred from goes-derived cloud properties. – J. Appl. Meteor. Climatol. **52**, 2009–2023.

Donat, M.G., T. Pardowitz, G.C. Leckebusch, U. Ulbrich, O. Burghoff, 2011: High-resolution refinement of a storm loss model and estimation of return periods of loss-intensive storms over Germany. – Natural Hazards and Earth System Sciences **11**, 2821–2833.

Done, J., G. Craig, S. Gray, P. Clark, M. Gray, 2006: Mesoscale simulations of organized convection: Importance of convective equilibrium. – Quart. J. Roy. Meteor. Soc. **132**, 737–756.

Dotzek, N., P. Groenemeijer, 2009: European Severe Weather Database, ESWD - Data format description. Technical Report 2099-01, ESSL Tech. Rep.. – Available at http://essl.org/media/publications/essl-tech-rep-2009-01.pdf.

Dotzek, N., P. Groenemeijer, B. Feuerstein, A.M. Holzer, 2009: Overview of ESSL's severe convective storms research using the European Severe Weather Database ESWD. – Atmos. Res. **93**, 575–586.

Gebhardt, C., S. Theis, M. Paulat, Z. Ben Bouallègue, 2011: Uncertainties in cosmo-de precipitation forecasts introduced by model perturbations and variation of lateral boundaries. – Atmos. Res. **100**, 168–177.

Groenemeijer, P., M. Kuehne, Z. Liang, N. Dotzek, 2009: New capabilities of the European Severe Weather Database. – 5th European Conference on Severe Storms, Landshut, Germany, 311–312.

Held, H., F.-W. Gerstengarbe, T. Pardowitz, J.G. Pinto, U. Ulbrich, K. Born, M.G. Donat, M.K. Karremann, G.C. Leckebusch, P. Ludwig, K.M. Nissen, H. Oesterle, B.F. Prahl, P.C. Werner, D.J. Befort, O. Burghoff, 2013: Projections of global warming-induced impacts on winter storm losses in the German private household sector. – Climatic Change **121**, 195–207.

Hengstebeck, T., D. Heizenreder, P. Joe, P. Lang, 2011: The mesocyclone detection algorithm of DWD. – 6th European Conference on Severe Storms, 3–7 October 2011, Palma de Mallorca, Spain.

Hohenegger, C., C. Schär, 2007: Predictability and Error Growth Dynamics in Cloud-Resolving Models. – J. Atmos. Sci. **64**, 4467–4478.

Hohl, T., H.H. Schiesser, 2000: Lightning patterns and their relation to the radar-derived hail kinetic energy. – Proc. European Tornadoes and Severe Storms conference, Toulouse, France.

Hohl, R., H.H. Schiesser, D. Aller, 2002: Hailfall: the relationship between radar-derived hail kinetic energy and hail damage to buildings. – Atmos. Res. **63**, 177–207.

Horvath, A., K. Wapler, F. Senf, H. Deneke, M. Diederich, J. Simon, S. Trömel, 2012: Lagrangian analysis of precipitation cells using satellite, radar, and lightning observations. – 2012 EUMETSAT Meteorological Satellite Conference, Sopot, Poland.

James, P., 2007: An objective classification method for Hess and Brezowsky Grosswetterlagen over Europe. – Theor. Appl. Climatol. **88**, 17–42.

Kain, J., M. Coniglio, J. Correia, A. Clark, P. Marsh, C. Ziegler, V. Lakshmanan, S. Miller, S. Dembek, S. Weiss, F. Kong, M. Xue, R. Sobash, A. Dean, I. Jirak, C. Melick, 2013: A Feasibility Study for Probabilistic Convection Initiation Forecasts Based on Explicit Numerical Guidance. – Bull. Amer. Meteor. Soc. **94**, 1213–1225.

Keil, C., F. Heinlein, G. Craig, 2014: The convective adjustment time-scale as indicator of predictability of convective precipitation. – Quart. J. Roy. Meteor. Soc. **140**, 480–490.

Kühnlein, C., C. Keil, G.C. Craig, C. Gebhardt, 2014: The impact of downscaled initial condition perturbations on convective-scale ensemble forecasts of precipitation. – Quart. J. Roy. Meteor. Soc. **140**, 1552–1562.

Kunz, M., M. Puskeiler, 2010: High-resolution assessment of the hail hazard over complex terrain from radar and insurance data. – Meteorol. Z. **19**, 427–439.

Lang, P., 2001: Cell tracking and warning indicators derived from operational radar products. – 30th Int. Conf. Radar Met., Munich, Germany, AMS Boston, 245–247.

Lang, T., S. Rutledge, 2002: Relationship between convective storm kinematics, precipitation, and lightning. – Mon. Wea. Rev. **130**, 2492–2506.

McCann, D., 1983: The Enhanced-V: A Satellite Observable Severe Storm Signature. – Mon. Wea. Rev. **111**, 887–894.

Mecikalski, J., K. Bedka, 2006: Forecasting Convective Initiation by Monitoring the Evolution of Moving Cumulus in Daytime GOES Imagery. – Mon. Wea. Rev. **134**, 49–77.

Mecikalski, J., W. MacKenzie, M. Koenig, S. Muller, 2010: Cloud-Top Properties of Growing Cumulus prior to Convective Initiation as Measured by Meteosat Second Generation. Part I: Infrared Fields. – J. Appl. Meteor. Climatol. **49**, 521–534.

Mecikalski, J., P. Watts, M. Koenig, 2011: Use of Meteosat Second Generation optimal cloud analysis fields for understanding physical attributes of growing cumulus clouds. – Atmos. Res. **102**, 175–190.

Peralta, C., Z. Ben Bouallègue, S. Theis, C. Gebhardt, M. Buchhold, 2012: Accounting for initial condition uncertainties in cosmo-de-eps. – J. Geophys. Res. **117**, (D07108).

Schultz, C., W. Petersen, L. Carey, 2009: Preliminary development and evaluation of lightning jump algorithms for the real-time detection of severe weather. – J. Appl. Meteor. Climatol. **48**, 2543–2563.

Schuster, S.S., R.J. Blong, K.J. McAneney, 2006: Relationship between radar-derived hail kinetic energy and damage to insured buildings for severe hailstorms in eastern australia. – Atmos. Res. **81**, 215–235.

Selz, T., G. Craig, 2014: Upscale error growth in a high-resolution simulation of a summertime weather event over Europe. – Mon. Wea. Rev., DOI: 10.1175/MWR-D-14-00140.1

Senf, F., F. Dietzsch, A. Huenerbein, H. Deneke, 2015: Characterization of initiation and growth of selected severe convective storms over Central Europe with MSG-SEVIRI. – J. Appl. Meteor. Climatol. **54** (1), 207–224.

Sieglaff, J., L. Cronce, W. Feltz, K. Bedka, M. Pavolonis, A. Heidinger, 2011: Nowcasting convective storm initiation using satellite-based box-averaged cloud-top cooling and cloud-type trends. – J. Appl. Meteor. Climatol. **50**, 110–126.

Siewert, C., M. Koenig, J. Mecikalski, 2010: Application of meteosat second generation data towards improving the nowcasting of convective initiation. – Meteor. Appl. **17**, 442–451.

Smith, P.L., 1999: Effects of imperfect storm reporting on the verification of weather warnings. – Bull. Amer. Meteor. Soc. **80**, 1099–1105.

Stensrud, D.J., L. Wicker, K. Kelleher, M. Xue, M. Foster, J. Schaefer, R.S. Schneider, S. Benjamin, S. Weygandt, J. Ferree, J. Tuell, 2009: Convective-scale warn-on-forecast system. – Bull. Amer. Meteor. Soc. **90**, 1487–1499.

Stephan, K., S. Klink, C. Schraff, 2008: Assimilation of radar-derived rain rates into the convective-scale model COSMO-DE at DWD. – Quart. J. Roy. Meteor. Soc. **134**, 1315–1326.

Trentmann, J., C. Keil, M. Salzmann, C. Barthlott, H.-S. Bauer, T. Schwitalla, M. Lawrence, D. Leuenberger, V. Wulfmeyer, U. Corsmeier, 2009: Multi-model simulations of a convective situation in low-mountain terrain in central europe. – Meteor. Atmos. Physics **103**, 95–103.

Vié, B., O. Nuissier, V. Ducrocq, 2011: Cloud-resolving ensemble simulations of mediterranean heavy precipitating events: Uncertainty on initial conditions and lateral boundary conditions. – Mon. Wea. Rev. **139**, 403–423.

Wapler, K., 2013: High-resolution climatology of lightning characteristics within Central Europe. – Meteor. Atmos. Physics **122**, 175–184.

Wapler, K., P. James, 2014: Thunderstorm occurrence and characteristics in Central Europe under different synoptic conditions. – Atmos. Res., DOI: 10.1016/j.atmosres.2014.07.011

Wapler, K., M. Göber, S. Trepte, 2012: Comparative verification of different nowcasting systems to support optimisation of thunderstorm warnings. – Adv. Sci. Res. **8**, 121–127.

Weingaertner, H., U. Schickedanz, M. Goeber, 2009: Wetterwarndienst. – promet **35**, 30–38.

Wicker, L., J. Kain, S. Weiss, D. Bright, 2005: A brief description of the supercell detection index. – Available at http://spc.noaa.gov/exper/Spring\T1\textbackslash_2005/SDI-docs.pdf.

Wilks, D., 2011: Statistical Methods in the Atmospheric Sciences. – Academic Press, Elsevier, 676 pp.

Wulfmeyer, V., A. Behrendt, H.-S. Bauer, C. Kottmeier, U. Corsmeier, A. Blyth, G. Craig, U. Schumann, M. Hagen, S. Crewell, P. Di Girolamo, C. Flamant, M. Miller, A. Montani, S. Mobbs, E. Richard, M. Rotach, M. Arpagaus, H. Russchenberg, P. Schlössel, M. König, V. Gärtner, R. Steinacker, M. Dorninger, D. Turner, T. Weckwerth, A. Hense, C. Simmer, 2008: The Convective and Orographically-induced Precipitation Study: A Research and Development Project of the World Weather Research Program for improving quantitative precipitation forecasting in low-mountain regions. – Bull. Amer. Meteor. Soc. **89**, 1477–1486.

Zimmer, M., G.C. Craig, C. Keil, H. Wernli, 2011: Classification of precipitation events with a convective response timescale and their forecasting characteristics. – Geophys. Res. Lett. **38**.

Zrnic, D.S., D.W.B.L.D., Hennington, 1985: Automatic detection of mesocyclonic shear with doppler radar. – J. Atmos. Oceanic Technol. **2**, 425–438.